DOI: 10.21062/mft.2025.066 http://www.journalmt.com

Research on Optimization Design and Processing Technology of Engine Intake System Based on NX and Fluent

Jun Zhang (0009-0001-5079-2435)*, Ruqian Gao (0009-0006-3810-0500), Yangfang Wu (0009-0008-5191-8328)
School of Engineering, Hangzhou City University, Hangzhou, 310015, China
*Email: jhzhang_2006@126.com

To design an engine intake system that complies with FSC racing regulations while achieving enhanced operational stability, this study conducts a comprehensive review of domestic and international research advancements in racing engine intake systems. Through computational fluid dynamics simulations performed in Workbench Fluent, critical structural parameters of the restrictor valve were optimized, resulting in a 12.06% improvement in outlet mass flow rate compared to the baseline design. A three-dimensional parametric model of the racing intake system was developed using Siemens NX platform. Taking the intake plenum chamber as a representative component, this research systematically analyzes the CNC machining process for the mold of the pressure stabilization chamber. The investigation encompasses toolpath generation, cutting simulation verification, and ultimately implements the optimized NC program on machining centers for physical manufacturing. The fabricated mold exhibits high dimensional accuracy and superior surface finish, providing both theoretical guidance and practical manufacturing references for intake system development. This integrated approach combining numerical optimization with advanced manufacturing techniques demonstrates significant potential for performance enhancement in motorsport engineering applications.

Keywords: Intake system, Fluent, NX, Processing technology

1 Introduction

Formula Student Combustion (FSC) is an automotive design and manufacturing competition for university students majoring in automotive engineering or related fields [1]. As the core component of the racing car, the engine critically impacts vehicle power, emissions, and fuel efficiency, with its intake system playing an indispensable role [2-3]. For safety compliance, FSC regulations strictly mandate the engine specifications: displacement <600 cc, a restrictor (inner diameter ≤20 mm) installed in the intake manifold, and an intake sequence defined as air filter - throttle - restrictor - intake manifold - pressure stabilization chamber - intake runner - engine [4]. Under the restrictor-induced flow area constraints, optimizing the intake system structure and refining manufacturing processes are essential to enhance airflow and boost power output.

Extensive research has been conducted globally on intake system optimization and machining techniques. Regarding intake design, Sharma et al. [5] obtained through experiments and calculations of the dimensional parameters of the components that the structural shape of the intake system has a significant impact on the airflow movement within the intake system and the flow rate at the outlet. Xie and Liu [6] took the engine intake pipe as the research object and employed the Fluent module of Ansys to simulate and analyze the airflow state. As a result, they achieved improved intake response characteristics and significantly enhanced the overall intake efficiency of the intake pipe. In machining process research, Mu et al. [7] investigated UG-based CNC programming for ultrasonic-assisted cutting of honeycomb cores, demonstrating that this approach significantly reduces manufacturing cycles through minimized non-cutting time and enhanced programming efficiency. The In-Process Workpiece (IPW) method proposed by Ma et al [8], significantly enhances the efficiency of dynamic characteristic prediction, achieving a 19.74% improvement in accuracy compared to existing methods, which validates its feasibility and superiority in machining processes.

Building on these findings, this study focuses on optimizing the Honda CBR600 engine intake system for collegiate racing teams, including throttle sizing, manifold redesign, and runner/plenum development. A 3D model was constructed in Siemens NX, followed by CNC toolpath planning and cutting simulations for the plenum mold. Physical molds were fabricated on machining centers, ensuring dimensional accuracy and surface quality.

2 Engine Intake System

The structure of the intake system is shown in Figure 1. It mainly consists of air filter, throttle, restrictor, plenum and intake manifold.

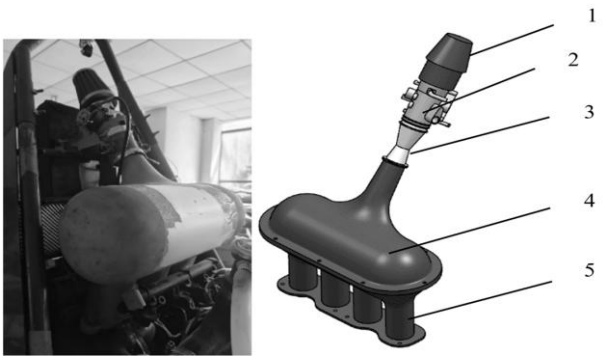

Fig. 1 *Composition of the intake system (1. Air filter, 2. Throttle, 3. Restrictor, 4. Plenum, 5. Intake manifold)*

The working principle of the system: After passing through the air filter, the gas passes sequentially through the throttle, restrictor, and diffuser into the plenum. The plenum stabilizes pressure and stores air volume. When the engine's intake valves open, the air-fuel mixture (atomized fuel and air) is inducted into the combustion chambers under negative pressure. The structural design of the intake system directly governs volumetric efficiency, thereby critically influencing engine power output and acceleration performance [9-10]. Consequently, the system must be optimized to maximize volumetric efficiency as a primary design criterion.

3 Intake System Design

3.1 Design Specifications and Requirements

Based on the Honda CBR600 engine, the intake system analyzes the factors influencing its charging efficiency, and completes the selection of the throttle opening diameter, as well as the design of the intake manifold, manifold pipe and plenum. Among them, the design requirements for the intake system in the FSC are as follows:

- A restrictor must be installed between the throttle and the engine, and its maximum inner diameter is 20 mm.
- The sole permitted intake sequence is throttle-restrictor-boosting device-engine.

3.2 Intake System Layout

In order to ensure that the engine has sufficient intake air volume and the intake resistance is at the lowest level, it is necessary to arrange the intake system reasonably. As shown in Figure 1, this depicts the layout design of the intake system for the racing car developed by our institute. The air filter is located on the top of the vehicle, positioned above the driver's helmet but below the main roll cage. Its opening faces the forward direction of the racing car, thereby increasing the windward area and enhancing the wind force during high-speed operation. This design effectively satisfies the intake requirements. The end of the intake manifold is connected to the center of the pressure stabilizing chamber with a smooth transition. This symmetrical structure ensures balanced airflow distribution across all four cylinders, thereby optimizing engine performance.

3.3 Restrictor Inlet/Outlet Taper Angle Optimization

As a critical component of the intake system, the restrictor is constrained by a minimum cross-sectional diameter of 20 mm [11]. To maximize gas flow, the design and optimization of its key structural parameters—inlet taper angle (ITA) and outlet taper angle (OTA)—are essential. Figure 2 illustrates the restrictor's 3D geometry, with a fillet transition applied at the minimum diameter section.

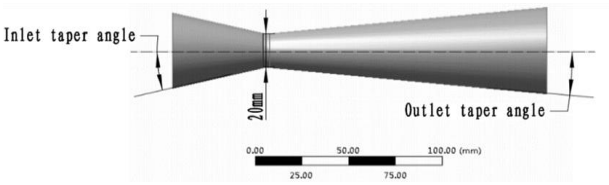

Fig. 2 *3D structural diagram of the flow-limiting valve*

A preliminary simulation was conducted on a restrictor model with an inlet cone angle of 16° and an outlet cone angle of 7°. The preprocessing phase employed ANSYS Meshing to generate a structured hexahedral-dominant mesh. Given the symmetrical structure of the model, half of the geometry was analyzed to enhance computational efficiency, as depicted in Figure 3(a). Boundary conditions were defined as follows: inlet (Pressure inlet) at 101325 Pa, outlet (Pressure outlet) at 97870 Pa, turbulence intensity of 5%, and turbulence viscosity ratio of 0.5. The generated mesh was subsequently imported into Fluent for further analysis. The boundary conditions corresponding to the engine's idle state were applied, and the solution was computed. Post-processing revealed the results, including an outlet mass flow rate of -0.0642402 kg/s. Additionally, the pressure contour, velocity vector, and gas flow streamline are illustrated in Figure 3.

In Figure 3, the maximum pressure occurs at the inlet end of the restrictor, with a value of 1.006×10^5 Pa; the minimum pressure occurs at the throat of the restrictor, with a value of 7.349×104 Pa; the maximum flow velocity occurs at the throat of the restrictor, with a value of 1.999×10^2 m/s, which conforms to the relevant principles and knowledge of fluid mechanics.

The structural optimization of the restrictor aims to enhance engine volumetric efficiency by maximizing the outlet mass flow rate. With inlet taper angle (ITA) and outlet taper angle (OTA) as input variables,

and outlet mass flow rate as the output parameter, a Response Surface Methodology (RSM) optimization was performed using ANSYS Workbench [12-13]. The input and output parameters were systematically integrated into the RSM module for analysis.

As illustrated in Figure 3, the angle between flow streamlines/vectors and the horizontal plane is smaller than that of the restrictor's outer boundary. This discrepancy suggests that reducing the OTA can increase outlet mass flow. Consequently, the OTA range was defined as 5°–7°, and the ITA range as 14°–18°. A Design of Experiments (DoE) approach generated nine design points (Table 1), systematically exploring parameter interactions to identify sensitivity trends.

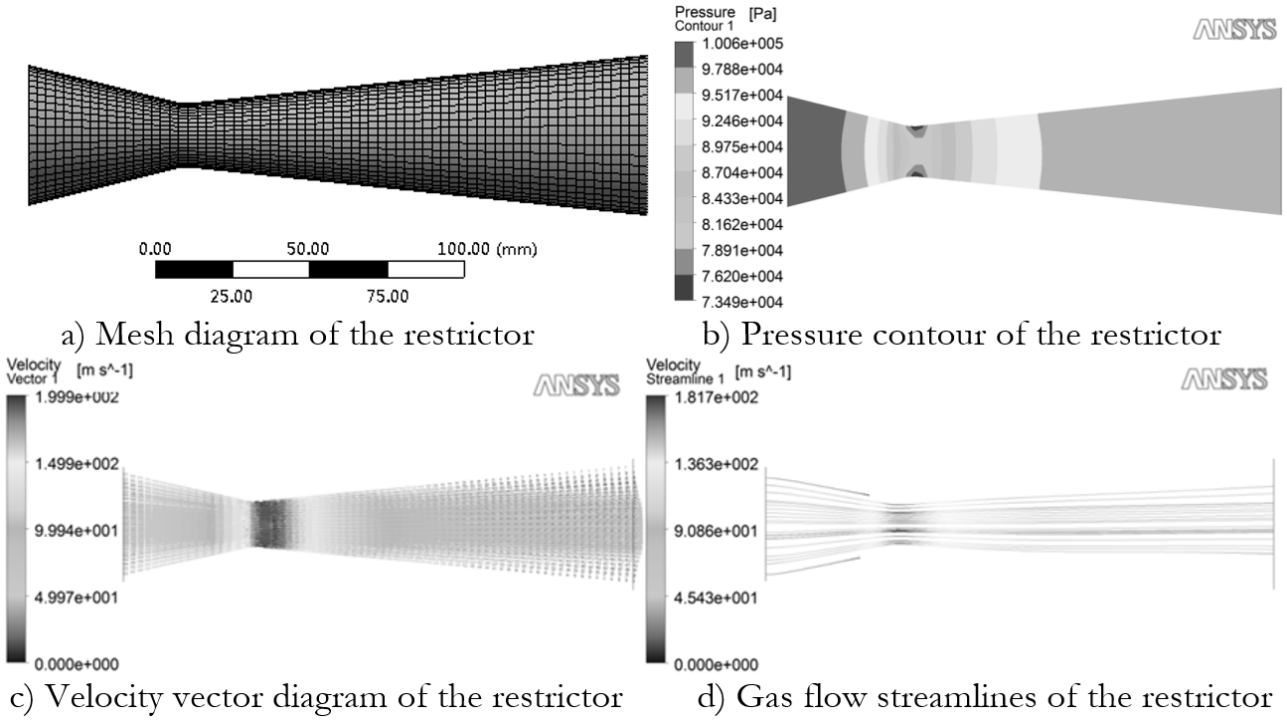

a) Mesh diagram of the restrictor b) Pressure contour of the restrictor

c) Velocity vector diagram of the restrictor d) Gas flow streamlines of the restrictor

Fig. 3 *Mesh Diagram, Pressure Contour, Velocity Contour, and Gas Flow Streamlines of the Restrictor*

Tab. 1 *Nine design points in the optimization process*

No.	Inlet Taper Angle (°)	Outlet Taper Angle (°)	Outlet Mass Flow Rate (kg/s)
1	14	5	-0.0715993
2	14	6	-0.0719891
3	14	7	-0.0653747
4	16	5	-0.0701039
5	16	6	-0.0701039
6	16	7	-0.0642402
7	18	5	-0.0663646
8	18	6	-0.0655345
9	18	7	-0.0625694

These design points enabled sensitivity analysis of parameters relative to the optimization objective (Figure 4), as well as the generation of corresponding response curves (Figures 5–6) and response surfaces (Figure 7).

Figure 4 illustrates the sensitivity of design variables to the objective function. The plotted data range reveals that the outlet taper angle (OTA) exerts a significantly stronger influence on the outlet mass flow rate than the inlet taper angle (ITA). Response curves in Figures 5 and 6 depict the impact trends of individual variables. As shown in Figure 5, the outlet mass flow rate decreases progressively with increasing ITA. Conversely, Figure 6 demonstrates that the mass flow rate initially rises with OTA but declines beyond 5.6°, indicating a nonlinear relationship.

The response surface plot (Figure 7) visualizes the combined effects of ITA (Y-axis) and OTA (X-axis) on the outlet mass flow rate (Z-axis). The maximum mass flow rate (-0.07199 kg/s) occurs near X=5.6°

(OTA) and Y=14° (ITA). Cross-referenced with Table 1, the optimal parameters were selected as OTA=6° and ITA=14°, balancing manufacturability and performance. This optimized configuration achieves a 12.06% improvement in mass flow rate compared to the baseline design, confirming the efficacy of the methodology.

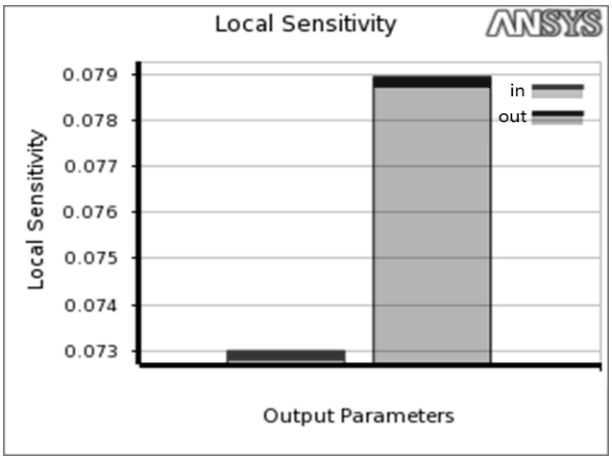

Fig. 4 *Sensitivity of design variables to the optimization objective*

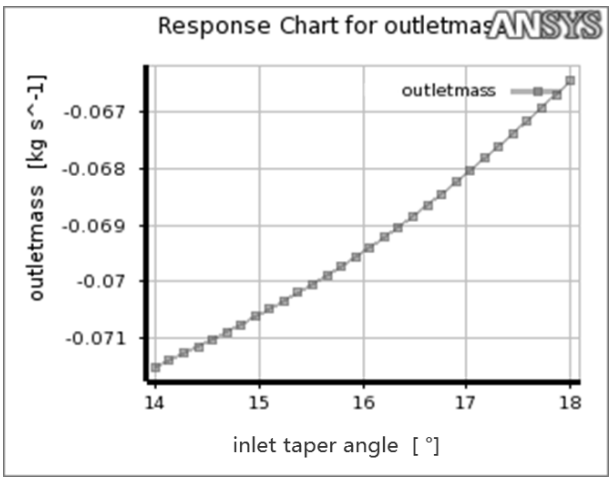

Fig. 5 *Response curve for inlet taper angle*

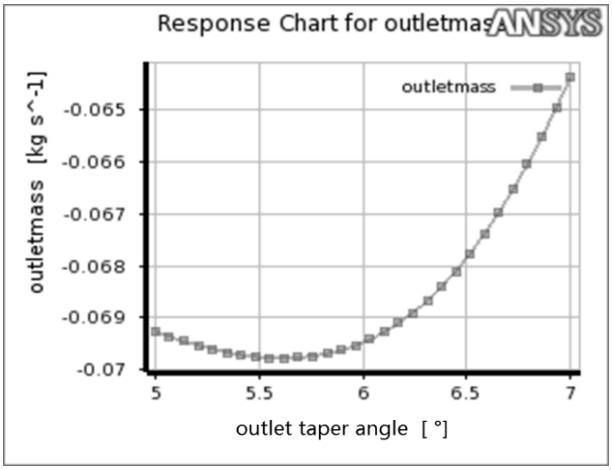

Fig. 6 *Response curve for outlet taper angle*

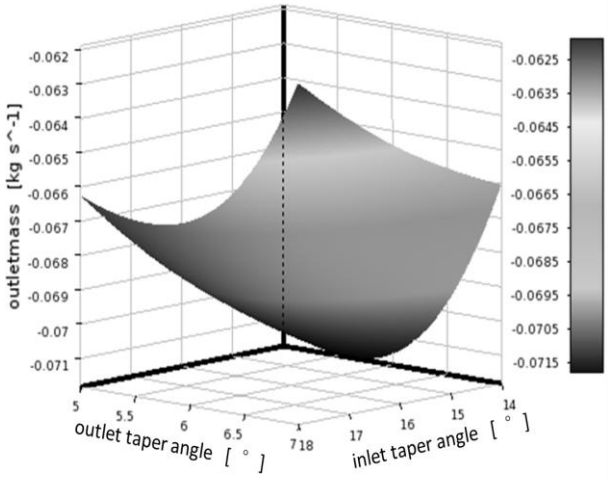

Fig. 7 *Response surface of parameters*

3.4 Additional Parameter Design of the Intake System

3.4.1 Throttle Bore Diameter

Under the FSC regulation constraints (mechanically controlled throttle), the bore diameter was determined through the fluid dynamics flow equation:

$$Q = C_d A \sqrt{\frac{2\Delta p}{\rho}} \tag{1}$$

Where:

C_d…The discharge coefficient (empirical range 0.6-0.7),

A…The flow area,

Δp…The pressure differential,

ϱ…The air density.

Reducing the bore diameter from D_1 =45 mm to D_2=40 mm decreased the flow area by 20.9% (calculated as $\Delta A/A_1=1-(D_2/D_1)^2$), thereby increasing localized flow velocity $v=Q/A$ to enhance throttle response. Consequently, a 40 mm bore diameter was selected.

3.4.2 Restrictor Structural Parameters

The intake manifold length was designed using Helmholtz resonance theory:

$$f_{\text{res}} = \frac{c}{2\pi}\sqrt{\frac{A}{VL}} \tag{2}$$

Where:

c=340 m/s…The sonic velocity,

$A=\pi D^2/4$…The cross-sectional area,

V…The plenum volume,

L…The manifold length.

Sensitivity analysis revealed:

- At L>250 mm, the resonance frequency f_{res} falls below idle excitation frequency ($f_{\text{idle}}=n_{\text{idle}}$ /120=66.7 Hz), causing high-speed airflow deficiency.

- At L<150 mm, f_{res} shifts to mid-range (f_{mid} =133 Hz), impairing low-speed torque.
- Multi-objective optimization yielded an optimal length L=200 mm.

3.4.3 Intake Runner Length: Calculated using the formula

$$L_1=30c/nq \quad (3)$$

Where:
c=340 m/s (speed of sound),
n=8000 r/min,
q=5 (pulsation coefficient),
yielding L_1=255 mm.

3.4.4 Plenum Volume

The plenum volume was determined by volumetric efficiency theory:

$$V_{\text{plenum}} \geq \frac{\dot{m}RT}{p\eta_v} \frac{1}{f_{ref}} \quad (4)$$

Where:
$\dot{m}$ =0.064 kg/s (standard air mass flow),
f_{ref}=133 Hz (characteristic frequency),
η_v=0.85 (empirical volumetric efficiency).

The minimum theoretical volume V_{min}=2.8 L was expanded to V=3.5 L with manufacturing tolerance. A cylindrical geometry (D=150 mm, L=200 mm) satisfies spatial constraints ($V=\pi D^2L/4$=3.53 L).

The finalized intake system parameters are summarized in Table 2.

Tab. 2 *Key parameters of the intake system*

Parameter	Value
Throttle Bore Diameter (mm)	40
Restrictor Inlet Taper Angle (°)	14
Restrictor Outlet Taper Angle (°)	6
Restrictor Total Length (mm)	200
Intake Runner Length (mm)	255
Plenum Volume (L)	3.5

4 Design and CNC Machining of the Plenum Mold

The plenum stabilizes pressure and stores energy within the intake system [14]. Its fabrication involves two stages:

- (1) Designing and CNC machining the plenum mold based on its 3D model;
- (2) Manufacturing the final plenum using carbon fiber fabric, resin, and the machined mold.

4.1 Machining Process of the Plenum Mold

The CNC machining process critically impacts part quality and efficiency [15]. The plenum mold (Figure 8) integrates the plenum and a truncated restrictor section to simplify machining.

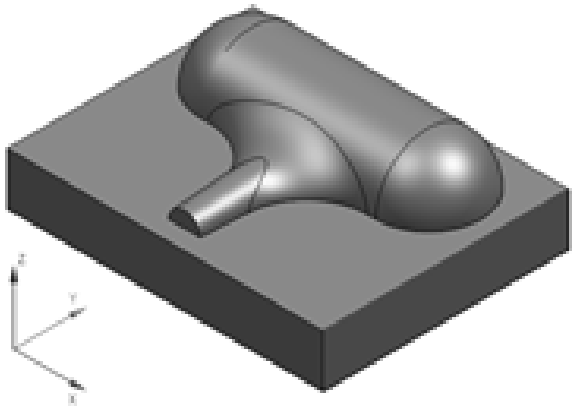

Fig. 8 *Plenum mold*

ABS was selected as the mold material. The optimized CNC process is detailed in Table 3.

Tab. 3 *CNC machining process for the plenum mold*

Step	Operation	Tool Type	Method
1	Roughing	Φ25 End Mill	Cavity Milling
2	Semi-Finishing (IPW*)	R3 Ball-Nose Mill	IPW Cavity Milling
3	Finishing	R2 Ball-Nose Mill	Fixed Contour Milling
*IPW: In-Process Workpiece			

4.2 NX CAM-Based CNC Programming

According to the numerical control (NC) machining process planning, the NC automatic programming flow of the pressure stabilizing cavity mold is shown in Figure 9.

Among them, the small planar body generated by roughing the mold is used as the blank body for semi-finishing the surface. This small planar body is called IPW (In Process Workpiece) [16]. Using IPW for processing can avoid re-cutting the already processed

areas and improve the overall processing efficiency [17], as shown in Figure 10.

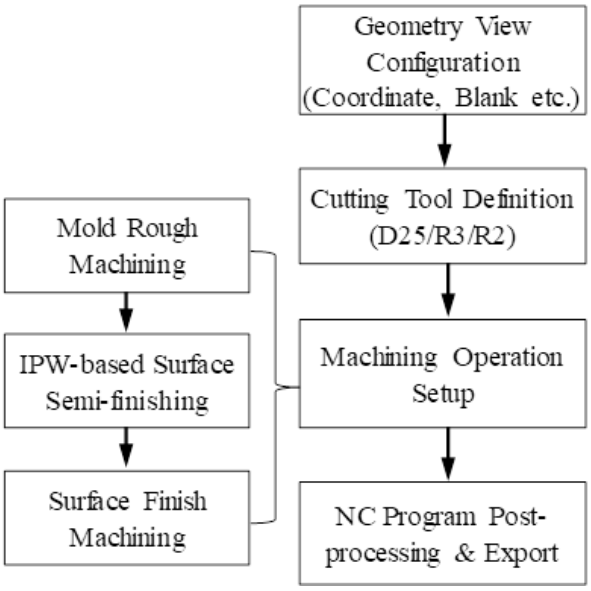

Fig. 9 *NX programming flowchart for the plenum mold*

In the Figure 10, Figure 10(a) represents the processing time without using IPW, and Figure 10(b) represents the processing time with IPW. It can be seen from the figure that the processing time is reduced by 5 minutes after using IPW, shortening the processing time of the process and improving the processing efficiency.

PROGRAM		09:43:08	
CAVITY_MILL	MILL_D25	04:54:51	MILL_ROUGH
CAVITY_MILL_1	BALL_MILL_R3	01:42:12	MILL_SEMI_FINISH
FIXED_CONTOUR	BALL_MILL_R2	03:05:29	MILL_FINISH

a) Machining time without IPW

PROGRAM		09:38:49	
CAVITY_MILL	MILL_D25	04:54:51	MILL_ROUGH
CAVITY_MILL_1	BALL_MILL_R3	01:37:53	MILL_SEMI_FINISH
FIXED_CONTOUR	BALL_MILL_R2	03:05:29	MILL_FINISH

b) Machining time with IPW

Fig. 10 *Comparison of machining time with and without IPW application*

4.3 CNC Milling Simulation

After the tool path programming for each process is completed, through tool path simulation, overcutting, tool collision and unreasonable path are checked, and the surface quality of the workpiece is observed to modify the parameters in the programming in time. The tool path and cutting simulation results are shown in Figure 11.

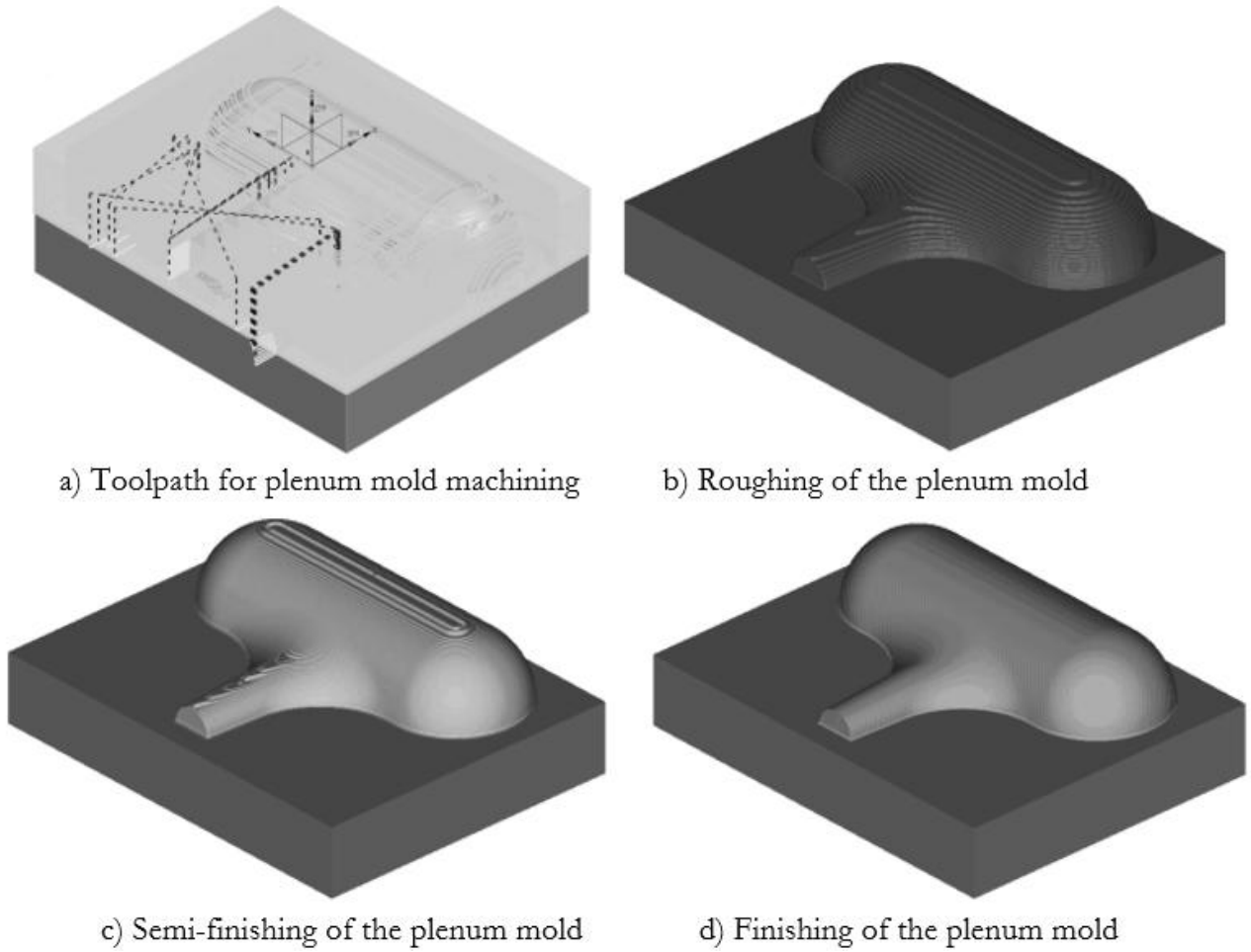

a) Toolpath for plenum mold machining

b) Roughing of the plenum mold

c) Semi-finishing of the plenum mold

d) Finishing of the plenum mold

Fig. 11 *Cutting simulation results of the plenum mold*

4.4 Post-Processing and NC Code Generation

Upon completion of tool path programming, the system generates a Cutter Location (CL) data file. As machine tool controllers cannot directly interpret CL data files, this intermediate output must undergo post-processing—a critical conversion stage that translates the geometrical information into machine-specific Numerical Control (NC) code. The post-processed NC program, containing axis movement commands and machining parameters compatible with the target CNC system, is subsequently saved in .ptp format. This standardized file format serves as the executable input for numerical control machine tools, facilitating seamless integration between CAM software and physical machining operations.

5 CNC Machining of the Plenum Mold

The experimental platform employs a VMC850 three-axis CNC machining center equipped with a FANUC 0i-MC control system. Mold fabrication for the pressure stabilization chamber was executed online via the machine's memory card interface. When machining ABS, two major issues, temperature rise and elastic deformation, are mainly considered [18-19]. Tool selection parameters prioritized three candidate materials: high-speed steel, cemented carbide, and diamond [20]. Since high-speed steel has better grinding performance and toughness [21], high-speed steel is selected for machining ABS. At the same time, to prevent excessive cutting force from causing local overheating and elastic deformation of the workpiece, the following machining parameters are adopted.

The multi-stage machining process commences with roughing operations conducted at 1,500 r/min spindle speed and 300 mm/min feed rate, implementing differential allowance allocation with zero bottom surface allowance and 0.5 mm sidewall retention [22]. This initial phase requires 1 hour to complete material stock removal. Subsequently, the semi-finishing stage employs elevated spindle speeds of 2,000 r/min, while maintaining 250 mm/min feed rates, uniformly preserving 0.3 mm machining allowance. Through implementation of IPW, this intermediate phase shortens the entire semi-finishing stage within 1.5 hours, improving the efficiency of semi-finishing stage. The final finishing operations utilize precision parameters of 2,000 r/min spindle rotation and reduced 200 mm/min feed rates, executing critical dimension control throughout the 2.0-hour finishing cycle [23].

a) Machined plenum mold b) Carbon fiber Plenum

Fig. 12 *Milled Plenum Mold and Final Carbon Fiber Component*

Figure 12(a) illustrates the machined pressure stabilization chamber mold on the VMC850. Subsequently, the carbon fiber solid of the pressure stabilization chamber was fabricated using carbon fiber cloth, resin, and other materials through processes such as surface application, vacuum infusion, and precision grinding. The resulting carbon fiber solid is presented in Figure 12(b).

6 Conclusion

This research focuses on the optimization design and manufacturing process of the engine intake system for FSC racing cars, aiming to enhance stability and volumetric efficiency under strict competition regulations. Based on Workbench Fluent, the critical structural parameters of the intake system, particularly the inlet and outlet cone angles of the restrictor valve, were optimized using the Response Surface Methodology (RSM). The optimal combination of parameters was determined as a 14° inlet cone angle and 6° outlet cone angle, resulting in a 12.06% improvement in the outlet mass flow rate. Furthermore, a three-dimensional model of the intake system was established using Siemens NX, and the numerical control (NC) machining process for the pressure-stabilizing cavity mold was systematically designed. By adopting the In-Process Workpiece (IPW) technique, the semi-finishing path was optimized, reducing the machining time by 5 minutes and improving overall efficiency. The mold was successfully fabricated on a VMC850 three-axis machining center with high dimensional accuracy and surface quality. The final carbon fiber pressure-stabilizing cavity was manufactured through vacuum-assisted resin infusion and polishing processes.

The integration of Fluent-based simulation and NX CAM-driven machining demonstrated significant advantages in enhancing design precision and production efficiency. The proposed methodology not only meets the technical requirements of FSC regulations but also provides a practical framework for the rapid development of high-performance intake systems. Future work will extend this approach to optimize other components of the intake system and conduct comprehensive performance tests under real-world operating conditions. Additionally, exploring advanced materials and hybrid manufacturing techniques could further improve the durability and lightweight characteristics of racing components, contributing to the overall competitiveness of the vehicle.

References

[1] LAI, N. Y. G., WONG, K. H., HALIM, D., MARETA, S., RAN, L., & CHEUNG, H. (2021). Learning through formula student electric: Students and staff perspectives. *2021 IEEE International conference on engineering, Technology & education (TALE), Wuhan, Hubei Province, China,*

IEEE, pp. 1-7. https://doi.org/10.1109/tale52509.2021.9678829

[2] MOHAMAD, B., KAROLY, J., ZELENTSOV, A. (2020). CFD modelling of formula student car intake system. *Facta Universitatis, Series: Mechanical Engineering*, Vol. 18, No. 1, pp.153-163. https://doi.org/10.22190/fume190509032m

[3] KARTHIKEYAN, K., DIVINE, S. A., JIBIN, J., THOMAS, S. J. (2023). CFD Analysis of Air Intake Manifold System to Improve the Efficiency of Student Formula Car. *International Journal of Vehicle Structures & Systems*, Vol. 15, No. 6, pp. 833-835. https://doi.org/10.4273/ijvss.15.6.18

[4] LI, L. (2024). *Formula Student China Competition Rules (2024 ed.)*. Society of Automotive Engineers of China.

[5] SHARMA, V., DHAUNI, S., CHAWLA, V. K. (2021). Design and manufacturing of air intake assembly for formula SAE vehicle. *Materials Today: Proceedings*, Vol. 43, No. Part 1, pp. 58-64. https://doi.org/10.1016/j.matpr.2020.11.209

[6] XIE, J., LIU, Z. (2022). Structural optimization on the design of an automobile engine intake pipe. *Journal of Theoretical and Applied Mechanics*, Vol. 60, No. 3, pp. 449-461. https://doi.org/10.15632/jtam-pl/151069

[7] MU, D., HU, X., YU, H., YU, B. (2021). Investigation of ultrasonic-assisted CNC cutting of honeycomb cores. *The International Journal of Advanced Manufacturing Technology*, Vol. 117, No. 3, pp. 1275-1286. https://doi.org/10.1007/s00170-021-07820-x

[8] MA, S., XIAO, J., LIU, H., LIU, S., TIAN, Y. (2023). Modeling and analysis for time-varying dynamics of thin-walled workpieces in mirror milling considering material removal. *Science China Technological Sciences*, Vol. 66, No. 7, pp. 1883-1898. https://doi.org/10.1007/s11431-022-2360-6

[9] LUO, K., HUANG, Y., HAN, Z., LI, Y., SHI, Y., LIU, W., TANG, C. (2022). Low-speed performance compensation of a turbocharged natural gas engine by intake strategy optimization. *Fuel*, Vol. 324, No, Part C, pp. 124748. https://doi.org/10.1016/j.fuel.2022.124748

[10] MASRI, J., AMER, M., SALMAN, S., ISMAIL, M., ELSISI, M. (2024). A survey of modern vehicle noise, vibration, and harshness: A state-of-the-art. *Ain Shams Engineering Journal*, Vol. 15, No. 10, pp. 102957. https://doi.org/10.1016/j.asej.2024.102957

[11] SATHISHKUMAR, A., SOUNDARARAJAN, R., KUMAR, S. R., KAARTHIK, G. M., VIGNESHWAR, R. R., ALI, L. F. (2024). Performance Enhancement through Air Intake Restrictor Tuning by Fluid Flow Analysis for Formula Vehicle. *SAE Technical Paper 2024-01-5202*. https://doi.org/10.4271/2024-01-5202

[12] LI, T., ZHANG, Y., LIANG, Y., YANG, Y., JIAO, J. (2021). Multiobjective optimization research on the response time of a pneumatic pilot-operated high speed on/off valve. *International Journal of Applied Electromagnetics and Mechanics*, Vol. 65, No. 1, pp. 109-127. https://doi.org/10.3233/jae-190074

[13] INDUDHAR, M. R., BANAPURMATH, N. R., RAJULU, K. G., PATIL, A. Y., JAVED, S., KHAN, T. Y. (2021). Optimization of piston grooves, bridges on cylinder head, and inlet valve masking of home-fueled diesel engine by response surface methodology. *Sustainability*, Vol. 13, No. 20, pp. 11411. https://doi.org/10.3390/su132011411

[14] BEYER, A., DI DOMENICO, D., BEATRICE, C., KULZER, A. C. (2025). High-pressure direct injection as enabling technology for high-power density hydrogen SI engines: Experimental analysis of the influence of jet-guided combustion regimes on efficiency and abnormal combustion. *Energy Conversion and Management*, Vol. 326, pp. 119497. https://doi.org/10.1016/j.enconman.2025.119497

[15] NTEMI, M., PARASCHOS, S., KARAKOSTAS, A., GIALAMPOUKIDIS, I., VROCHIDIS, S., KOMPATSIARIS, I. (2022). Infrastructure monitoring and quality diagnosis in CNC machining: A review. *CIRP Journal of manufacturing Science and Technology*, Vol. 38, pp. 631-649. https://doi.org/10.1016/j.cirpj.2022.06.001

[16] WANG, Y., JI, L., DONG, J., LIU, M., LIU, J. (2023). Research on Continuous Machining Strategy for Five-Axis Machine Tool: Five-Axis Linkage to Four-Axis Linkage. *Applied Sciences*, Vol. 13, No. 12, pp. 7038. https://doi.org/10.3390/app13127038

[17] EHSAN, S., ALI, M. A., KHAN, S. A., SANA, M., YASIR, M., ANWAR, S., FAROOQ, M. U. (2024). Understanding the effects of cutting conditions on vibrations, surface integrity, machining temperature and tool wear mechanisms

in end milling of AISI D2 Steel. *Tribology International*, Vol. 198, pp. 109894. https://doi.org/10.1016/j.triboint.2024.109894

[18] KANNAN, S., RAMAMOORTHY, M. (2020). Mechanical characterization and experimental modal analysis of 3D Printed ABS, PC and PC-ABS materials. *Materials Research Express*, Vol. 7, No. 1, pp. 015341. https://doi.org/10.1088/2053-1591/ab6a48

[19] HE, F., KHAN, M., ALDOSARI, S. (2022). Interdependencies between dynamic response and crack growth in a 3D-printed acrylonitrile butadiene styrene (ABS) cantilever beam under thermo-mechanical loads. *Polymers*, Vol. 14, No. 5, pp. 982. https://doi.org/10.3390/polym14050982

[20] MARTINS, P. S., JÚNIOR, P. A. A. M., CARNEIRO, J. R. G., BA, E. C. T., VIEIRA, V. F. (2022). Study of Diamond-Like Carbon coating application on carbide substrate for cutting tools used in the drilling process of an Al–Si alloy at high cutting speeds. *Wear*, Vol. 498-499, pp. 204326. https://doi.org/10.1016/j.wear.2022.204326

[21] ABOLOJE, A. E., SADA, S. O. O., EKPU, M., EYENUBO, J. (2024). Evaluation of the optimal cutting performance of high-speed steel and tungsten carbide cutting tools in the machining of AISI 304 steel. *The International Journal of Advanced Manufacturing Technology*, Vol. 130, No. 7, pp. 3609-3617. https://doi.org/10.1007/s00170-023-12909-6

[22] SEMENOV, S., MIKHAILOV, E., SPIVAK, O., DIŽO, J., BLATNICKÝ, M., BUČKO, M. (2025). Features of Locomotive Adhesive Mass Utilization in a Braking Mode. *Manufacturing Technology*, Vol. 25, No. 3, pp. 374-382. Doi: 10.21062/mft.2025.040

[23] WANG, L., HAN, L., HE, L., WANG, K., ZHU, X. (2024). Study on the Mechanism of Improving Surface Roughness of Gray Cast Iron Machining by Wiper Inserts. *Manufacturing Technology*, Vol. 24, No. 3, pp. 478-482. Doi: 10.21062/mft.2024.049